Ultraclean and large-area monolayer hexagonal boron nitride on Cu foil using chemical vapor deposition

Ultraclean and large-area monolayer hexagonal boron nitride on Cu foil using chemical vapor deposition

Yao Wen[1], **Xunzhong Shang**[2], **Ji Dong**[1], **Kai Xu**[1], **Jun He**[1] and **Chao Jiang**[1]

[1] CAS Key Laboratory for Standardization and Measurement for Nanotechnology, National Center for Nanoscience and Technology, Beijing 100190, People's Republic of China
[2] Faculty of Materials Science and Engineering, Hubei University, Wuhan 430062, People's Republic of China

E-mail: jiangch@nanoctr.cn

Abstract

Atomically thin hexagonal boron nitride (h-BN) has been demonstrated to be an excellent dielectric layer as well as an ideal van der Waals epitaxial substrate for fabrication of two-dimensional (2D) atomic layers and their vertical heterostructures. Although many groups have obtained large-scale monolayer h-BN through low pressure chemical vapor deposition (LPCVD), it is still a challenge to grow clean monolayers without the reduction of domain size. Here we report the synthesis of large-area ($4 \times 2 \, cm^2$) high quality monolayer h-BN with an ultraclean and unbroken surface on copper foil by using LPCVD. A detailed investigation of the key factors affecting growth and transfer of the monolayer was carried out in order to eliminate the adverse effects of impurity particles. Furthermore, an optimized transfer approach allowed the nondestructive and clean transfer of the monolayer from copper foil onto an arbitrary substrate, including a flexible substrate, under mild conditions. Atomic force microscopy indicated that the root-mean-square (RMS) roughness of the monolayer h-BN on SiO_2 was less than 0.269 nm for areas with fewer wrinkles. Selective area electron diffraction analysis of the h-BN revealed a pattern of hexagonal diffraction spots, which unambiguously demonstrated its highly crystalline character. Our work paves the way toward the use of ultraclean and large-area monolayer h-BN as the dielectric layer in the fabrication of high performance electronic and optoelectronic devices for novel 2D atomic layer materials.

S Online supplementary data available from stacks.iop.org/NANO/26/275601/mmedia

Keywords: hexagonal boron nitride, monolayer, ultraclean, large-area, highly crystalline, copper foil

(Some figures may appear in colour only in the online journal)

1. Introduction

Hexagonal boron nitride (h-BN), a honeycomb structure, is a promising insulating material with a direct band gap of 5.2–5.97 eV [1–3]. It is an ideal substrate in van der Waals epitaxy, especially for graphene devices, as its surface is atomically smooth and free of dangling bonds and charge traps [4], so the mobility of graphene can be increased by an order of magnitude [5, 6]. Atomic layers of WS_2 have been fabricated on high quality h-BN [7], as well as crystalline films of organic molecules such as rubrene, dioctylben-zothienobenzothiophene (C_8-BTBT) [8, 9]. Furthermore, h-BN has many excellent properties, including high temperature stability and good mechanical and thermal conductivity [10–13].

There are many ways to synthesize monolayer and few layer h-BN. Mechanical exfoliation is a simple and effective method [14], but it is extremely difficult to obtain large-area

flakes for use in practical optoelectrical devices. Monolayer h-BN has been successfully synthesized by ultra-high vacuum chemical vapor deposition (UHVCVD) on single-crystal noble and transition metals such as Ru, Rh, Rt, Pt, Ni, Pd, Ag, and Cu [15–22] Inspired by the recent progress of graphene synthesis, the growth of wide area h-BN has been investigated with various polycrystalline metals such as Ni, Co, Pt, and Cu using LPCVD or atmospheric pressure chemical vapor deposition (APCVD) [23–27]. The synthesis on Pt has been very successful using LPCVD systems. The bubbling-based transfer method has been demonstrated to be a simple and effective way to transfer h-BN from platinum onto an arbitrary substrate, and it allows the Pt foil to be recycled. However, Pt foils are very expensive and may be easily damaged in the process of transfer, so it is almost impossible to scale up for mass production. In contrast, copper has many advantages, as it is cheap, readily available as a single-crystal material, and easy to process into a flat surface via simple electrochemical polishing. As a result, synthesis of high quality h-BN on copper foils is promising because of its cost advantage and potential ability for mass production. Great efforts have been implemented to synthesize high quality h-BN so far. Two to five atomic layers of h-BN have been synthesized successfully over large areas [24], as well as interrupted monolayers on Cu foil with multiple layers being formed on some sites [25]. Recently, growth of large single-crystalline monolayer h-BN on electropolished copper has been reported [28] However, to obtain monolayers without surface impurities is very difficult, and the origin of those impurities remains uncertain. Although the synthesis of large-area unbroken monolayers of h-BN without surface impurities on copper foil is a great challenge, it is extremely necessary when integrating with other components or implementing a practical device.

Here, we report a method of synthesizing monolayer h-BN on copper foil using LPCVD. A detailed investigation into the influence of impurity particles was performed. Furthermore, we optimized the electrochemical bubble method, using methylene chloride as a solvent for polymethyl methacrylate (PMMA). The entire transfer process was rapid and feasible under mild conditions. As a result, PMMA residue could be considerably removed by methylene chloride without thermal annealing. Nondestructive, clean, and rapid transfer of monolayer h-BN was achieved, and this method may be readily applied to transfer various 2D materials grown on metals onto diverse substrates. We have achieved large-area, unbroken monolayer h-BN without any surface impurities even after a substrate transfer. Furthermore, its RMS roughness and crystallinity are among the best reported for CVD growth, and comparable to that of the growth on platinum foil.

2. Experimental details

2.1. Preparation method

Figure S1 is a schematic diagram of the LPCVD system (supporting information, figure S1). Ammonia borane (NH_3-

BH_3) (97% purity, from Sigma-Aldrich), stable in an atmospheric environment, was used as the precursor. It was placed in a small quartz tube (10 mm in diameter) in front of the tube furnace (50 mm in diameter). The quartz tube outlet was blocked by quartz wool as a filter. Copper (99.98%, 25 μm thick) was used as a metal catalyst substrate. After the pretreatment, a copper foil was placed in the center of the tube furnace, and then annealed at 1050 °C in flowing hydrogen gas (15 sccm) for 40 min to obtain copper grains and a smooth surface. The precursor was heated to 100 °C, and decomposed to hydrogen, monomeric aminoborane, and borazine ((HBNH)3; gas) [29]. Borazine diffused from the filter into the furnace. Filters were used to prevent the BN nanoparticles from diffusing into the furnace [30]. After growth, the tube furnace was quickly cooled down to room temperature.

2.2. Pretreatment of copper

Copper foil (99.98% pure and 25 μm thick) was soaked in acetone and ethanol for 10 min to remove organic impurities. It was washed with 10% acetic acid for 10 min, rinsed several times with deionized water to remove residues, then electropolished at 8 V under constant flow for 90 s in an electrolyte composed of 330 ml deionized water, 167 ml ortho-phosphoric acid, 167 ml ethanol, 33 ml isopropyl alcohol, and 3.3 g urea [28]. Finally, it was washed with deionized water and dried with nitrogen gas. The foil was then annealed at 1050 °C for 40 min under a flow of 15 sccm of H_2 gas to grow copper grains and obtain a smooth surface.

2.3. Transfer

The h-BN/Cu was spin-coated with PMMA (5%, methylene chloride) at 3000 rpm for 1 min. Then, PMMA/h-BN/Cu without baking was used as a cathode immersed in an aqueous solution of 0.1 M NaOH, while Au was used as an anode. The PMMA/h-BN was detached from the copper at 10 V under a constant flow within 1 min. It was then rinsed in deionized water for about 2 min, transferred onto a SiO_2/Si or polyimide substrate, and dried at 50 °C for 3 min. Finally, PMMA was completely removed with dichloromethane at 50 °C. Figure 1(a) is a photograph of h-BN on a Cu foil of size 2×4 cm^2. Figure 1(b) shows the h-BN transferred onto the SiO_2/Si substrate within the white dashed line. Figures 1(c) and (d) and S2(a) and S2(b) show AFM images of the h-BN on the SiO_2/Si substrate, as well as the height profile within the yellow dashed line in figure 1(b). It can be seen that we have obtained a large-area monolayer of h-BN. The wrinkles in the film, caused by the negative thermal expansion coefficients, are clearly visible in the AFM image [25].

2.4. Characterization

The morphology of the monolayer h-BN was characterized by optical microscopy (Leica DM4000M microscope), field emission scanning electron microscopy (Hitachi S4800), AFM (Dimension 3100), Raman spectroscopy (Renishaw
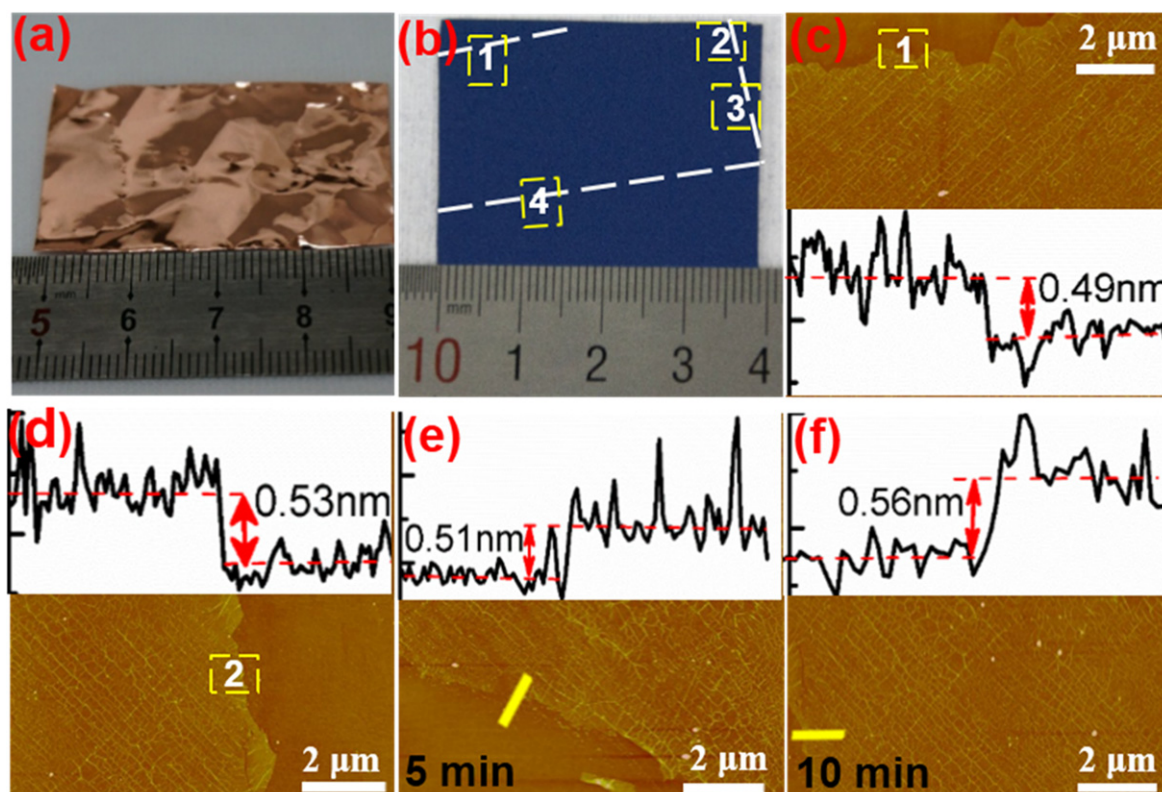
Figure 1. (a) Photograph of h-BN on a Cu foil of size 2×4 cm^2. (b) Photograph of monolayer h-BN on the SiO$_2$/Si substrate within the white dashed line. (c), (d) AFM images of the h-BN on the SiO$_2$/Si substrate and the height profile within the yellow dashed line shown in (b). (e), (f) AFM images of the h-BN on the SiO$_2$/Si substrate after it was grown on Cu foil for different growth periods of (e) 5 min, (f) 10 min.
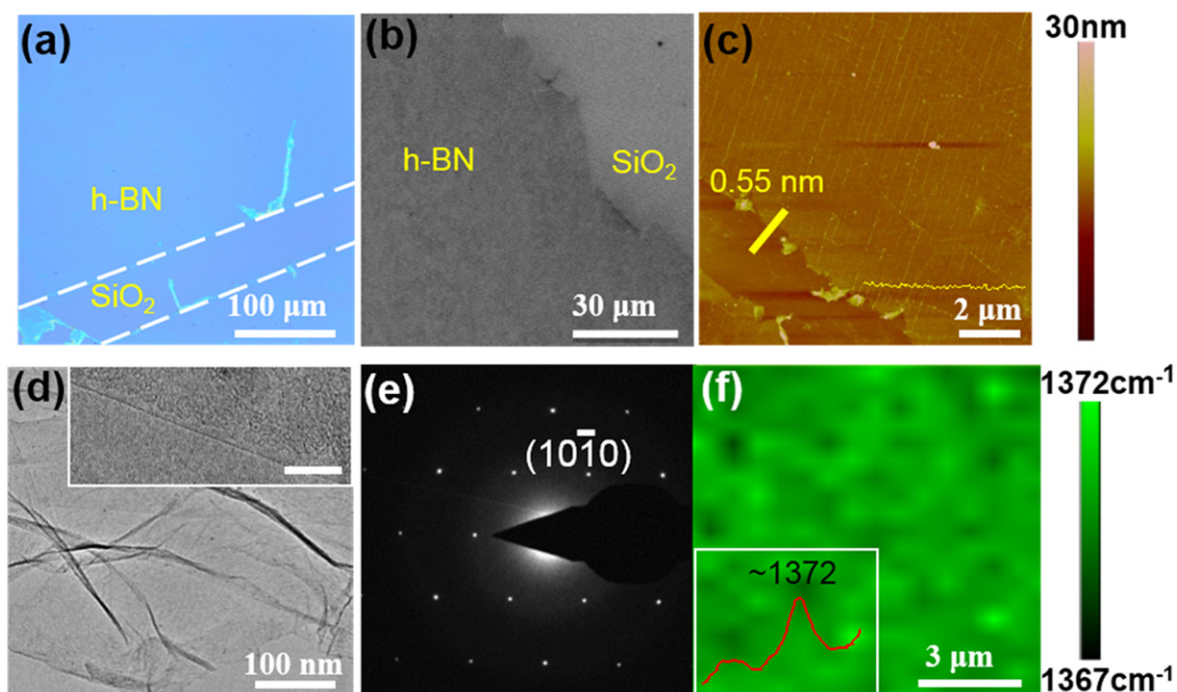

Figure 2. Images of monolayer h-BN on SiO$_2$/Si substrate observed by (a) optical microscopy, (b) SEM, and (c) AFM. (d) A low-magnification TEM image of monolayer h-BN on a quantifoil TEM grid; the inset is an HRTEM image of the monolayer edge; scale bar is 5 nm. (e) SAED diffraction pattern of monolayer h-BN. (f) Raman mapping of monolayer h-BN corresponding to the E$_{2g}$ vibration mode; the inset is the Raman spectrum.
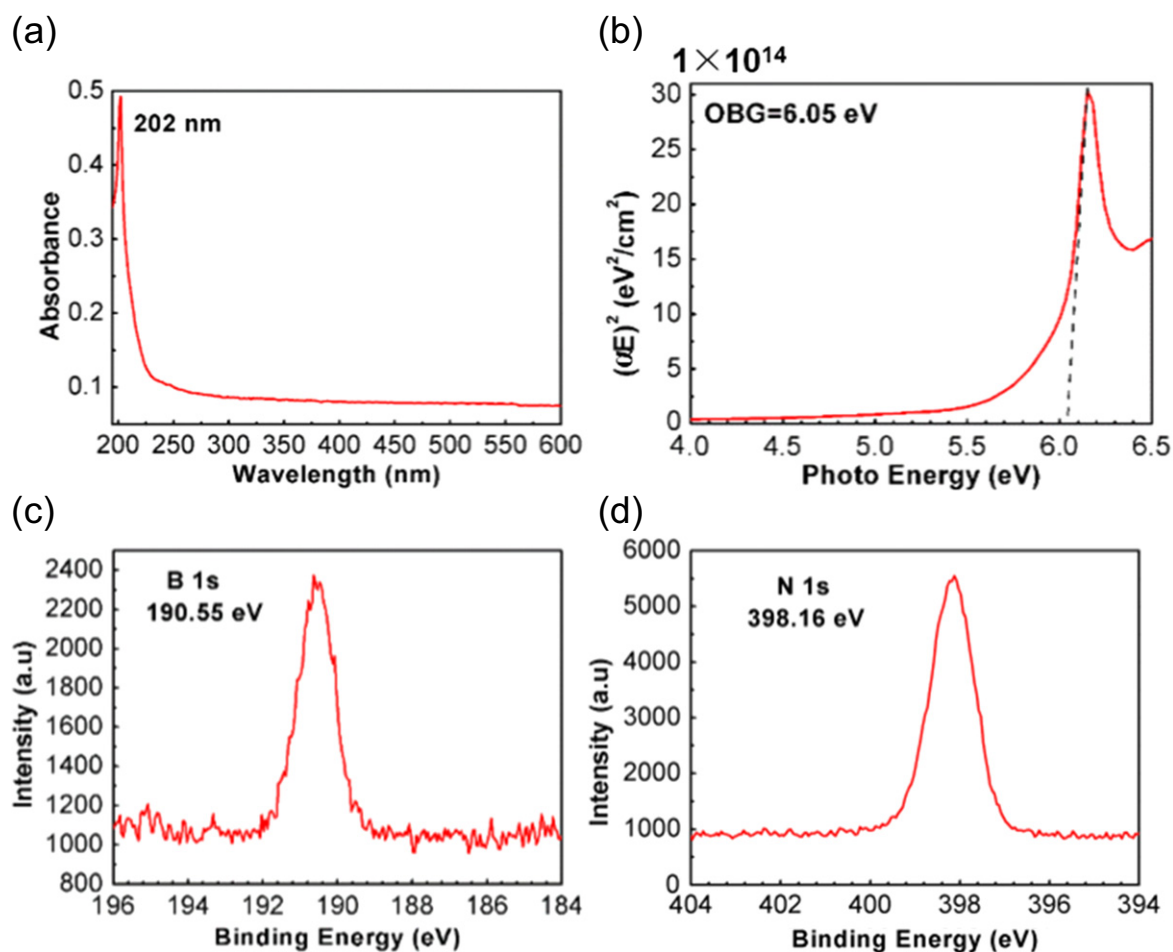
(a)

(b)

(c)

(d)

Figure 3. (a) UV–visible absorption spectrum of monolayer h-BN. (b) Optical band gap measurement. (c), (d) XPS spectrum of monolayer h-BN transferred onto a SiO_2/Si substrate: (c) B 1 s spectrum and (d) N 1 s spectrum.

InVia, 532 nm excitation laser), transmission electron microscopy (TEM), and high-resolution transmission electron microscopy (HRTEM), with a selected area electron diffraction (SAED) attachment on the TEM microscope (Tecnai G2 F20 U-TWIN). The UV–visible absorption spectrum was acquired using a Lambda 950 spectroscope; x-ray photon emission spectroscopy (XPS) was carried out on an ESCA-LAB250Xi facility.

3. Results and discussion

Within 5 min, borazine was adsorbed on the copper surface, forming a complete monolayer of h-BN. Due to the weak binding energy of the precursor molecules with the h-BN at our growth temperature, extra borazine molecules were rapidly desorbed back into the gas phase [31]. The grown h-BN monolayer constituted an inert layer, preventing further upward growth. Even when the growth time was extended to 10 min or longer, the thickness of the h-BN was still less than 0.56 nm, as shown in figures 1(e) and (f). This means that after the first layer has been grown, the number of layers do not increase further with time because growth of the second layer is restricted.

Figure 2(a) shows an optical microscope image of monolayer h-BN on a SiO_2 (300 nm)/Si substrate after the whole transfer process. The optical contrast is uniform, and the h-BN region in the figure is practically indistinguishable, without any curliness at its edges, indicating that the monolayer is very clean and uniform [32]. To verify this unambiguously, SEM and AFM were also employed and the images are shown in figures 2(b) and (c). No obvious residues can be seen on the h-BN surface. The RMS roughness (the yellow line) is shown in the inset of figure 2(c), where we find that the RMS roughness is less than 0.269 nm for areas with fewer wrinkles. The thickness of the monolayer is less than 0.55 nm, which matches well with previous reports [31, 32], and the area is as large as 100 μm^2. Figure 2(d) shows an image on a quantifoil TEM grid; an ultraclean and unbroken surface is again confirmed. The authenticity of monolayer h-BN can be further determined by analyzing the contrast edge of the layer in the inset of figures 2(d). Figure 2(e) shows the SAED pattern, wherein the hexagonally arranged spots can be indexed with (10$\bar{1}$0) diffraction, clearly revealing the high crystallinity of the h-BN [31]. Figure 2(f) indicates Raman mapping corresponding to the E_{2g} vibration mode, while the inset shows the Raman spectrum. Compared with bulk h-BN, the peak of the
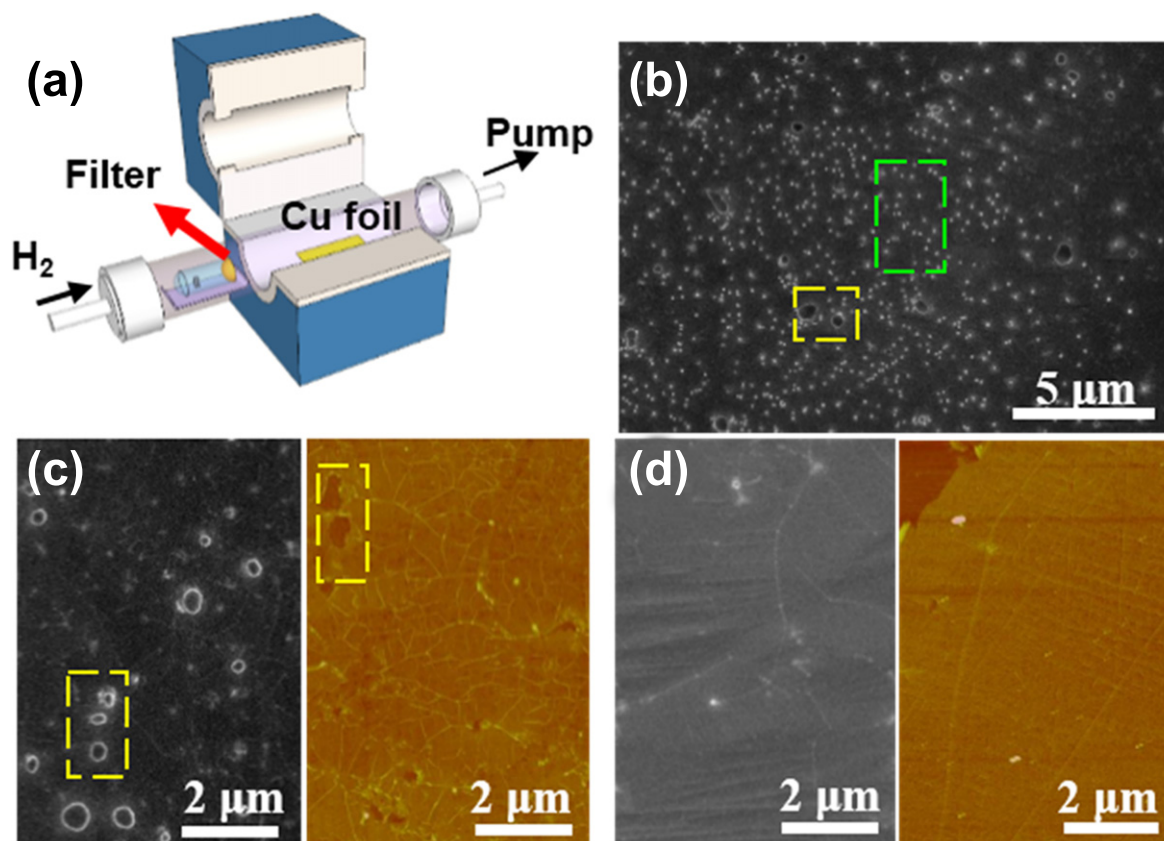
Figure 4. (a) Schematic diagram of LPCVD system. (b) SEM images of monolayer h-BN on a Cu substrate. The white dots correspond to BN nanoparticles within the green dashed line, and the large black dots correspond to impurity particles within the yellow dashed line. (c) Left: SEM image of h-BN grown on copper utilizing a filter. Right: AFM image of h-BN on the SiO_2/Si substrate. (d) Left: SEM image of h-BN grown on pretreated copper utilizing a filter. Right: AFM images of h-BN on the SiO_2/Si substrate.

monolayer h-BN is shifted to a higher frequency range, from 1368 to 1373 cm^{-1} [31, 33, 34]. The fluctuation of the E_{2g} vibration mode is probably due to local strain concentrated at the wrinkles [32, 33]. For our samples, most of the E_{2g} vibration modes corresponded to an energy range of 1370 to 1372 cm^{-1}, again indicating that our sample was really monolayer over a large region.

By transferring the monolayer h-BN to a piece of quartz glass, we could estimate its optical band gap E_g using UV–visible absorption spectroscopy and the formula for direct band gap semiconductors. A strong absorption peak is observed at 202 nm, as shown in figure 3(a). The absorption coefficient can be expressed as $\alpha = C\,(E–E_g)^{1/2}/E = A/d$, where C is a constant, E is the photon energy, A is the optical absorbance, and d is the film thickness, (taken to be 0.55 nm). We plot $(\alpha E)^2$ versus E, as shown in figure 3(b), and extrapolate the rising edge of the energy dispersion curve to the E axis. When $(\alpha E)^2$ is equal to 0, the corresponding value of E is equal to the optical band gap energy E_g, which is 6.05 eV in our work [28]. In fact, this matches previous theoretical predictions (6.0 eV) quite well [31]. In previous reports, the values were 5.94, 5.84, and 5.2 to 5.4 eV, for a bilayer, a few layers, and bulk h-BN, respectively [1–3, 35]. The band gap value of monolayer h-BN is slightly larger than for the bilayer and few layers, but much larger than for bulk h-BN, which

can be attributed to the fact that there is no layer–layer interaction [23, 24]. To determine the ratios of elements B and N, XPS was used to characterize the elementary composition of our monolayer h-BN. The binding energies of B 1 s and N 1 s are 190.55 and 398.16 eV, as shown in figures 3(c) and (d), respectively. These values are similar to those of previous reports [28, 31]. An elemental analysis shows the atomic percentage ratio of B to N to be about 1:1.02, indicating ideal chemical stoichiometry.

We also performed a systematic investigation on the origin and influence of the impurity particles. Especially, great efforts were made to eliminate various kinds of impurities that usually appear on the copper surface during annealing. When h-BN is grown on copper foil, there exist two kinds of impurities: BN nanoparticles and impurity particles arising from the CVD growth. Figure 4(a) is a schematic diagram of the LPCVD system. Figure 4(b) shows SEM images of monolayer h-BN on a copper substrate. These two kinds of impurities can be easily distinguished. The impurity particles are about 50–100 nm in diameter and larger than the BN nanoparticles that were formed by monomeric aminoborane. As shown in figure 4(a), a mass of quartz cotton (of fiber diameter ∼1–10 μm) was used as a filter, which prevented the BN nanoparticles from reaching the surface of the h-BN. The copper foil was annealed at 1050 °C in flowing
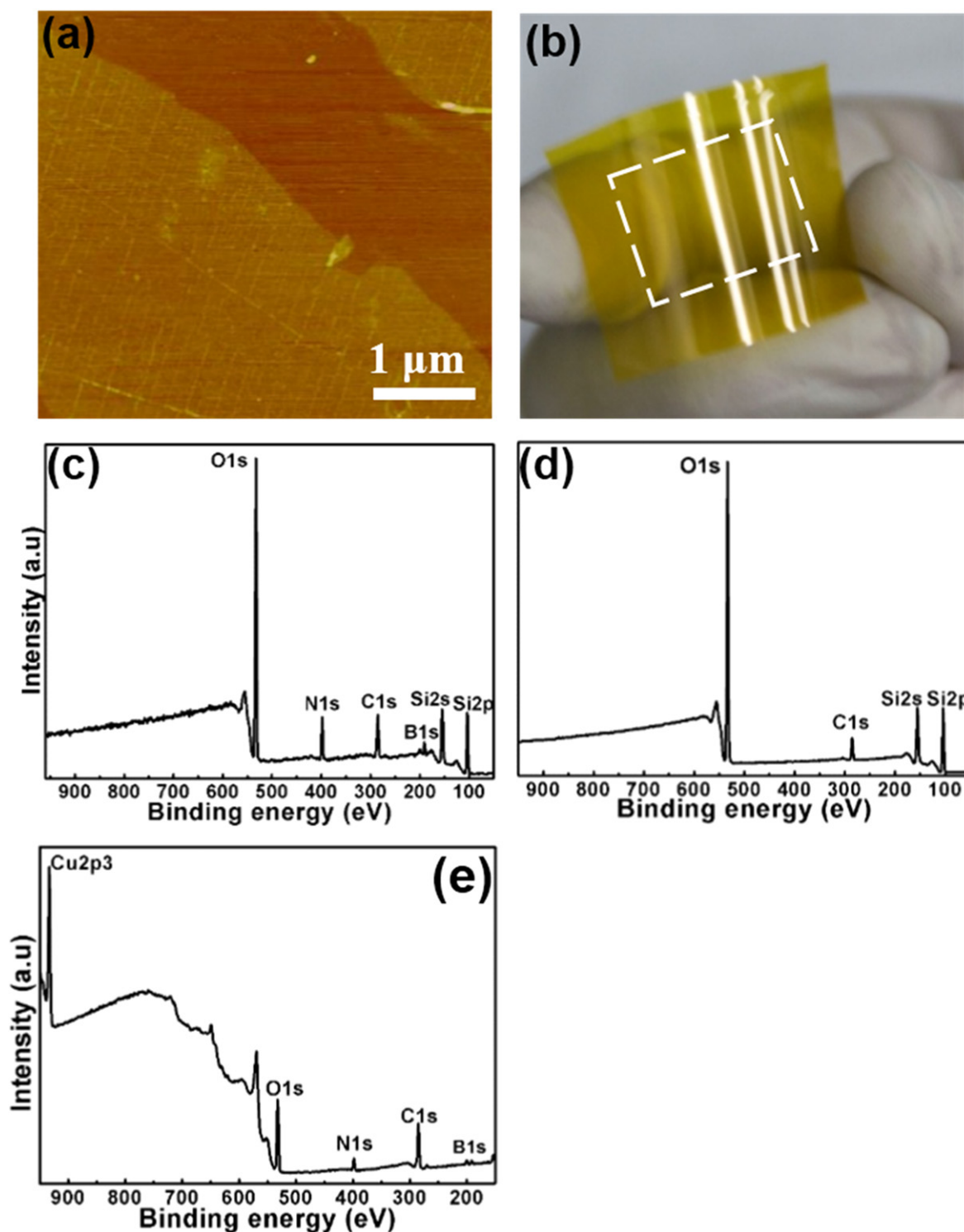
Figure 5. (a) AFM image of monolayer h-BN on a SiO_2/Si substrate. (b) Photograph of monolayer h-BN transferred onto a polyimide substrate. XPS spectrum of (c) monolayer h-BN transferred onto a SiO_2/Si substrate. (d) A SiO_2/Si substrate. (e) A h-BN/Cu foil.

hydrogen gas (15 sccm) for 40 min. Then, SEM was used to characterize the surface topography of the annealed copper. Many impurity particles could be clearly observed, of sizes ranging from 0.5 to 2 μm (see supporting information, figure S3(a)). However, after the copper foil was pretreated with acetic acid and electrochemical polishing, the impurities were notably decreased (supporting information, figure S3(b)).

The effects of the impurity particles on the growth of monolayer h-BN were then studied. Figure 4(c) (left) shows the SEM image of h-BN grown on copper utilizing a filter, while figure 4(c) (right) corresponds to an AFM image of monolayer h-BN on SiO_2/Si. Many holes between 0.5–2 μm in size could be observed, and the density of holes was similar to that of the impurity particles. Therefore, we have reason to

believe that the holes were caused by incomplete growth. The size of the impurity particles was much larger than the thickness of the monolayer h-BN. In contrast, copper pre-treated with acetic acid and electrochemical polishing led to much better morphology of the h-BN, as shown in figure 4(d) (left), with no obvious impurity particles [36]. Figure 4(d) (right) corresponds to AFM images of h-BN on SiO₂/Si. Compared with the untreated copper, the holes in the monolayer disappeared.

An optimized electrochemical bubbling method has been successfully applied to transfer monolayer h-BN from copper foil onto an arbitrary substrate [37–40]. We found that PMMA film fabricated by using methylene chloride as a solvent (5%, methylene chloride) was tough enough to keep the monolayer intact during the entire transfer process. In our method, the electrochemical bubble treatment was immedi-ately performed after the spin coating of PMMA without any baking. Hexagonal boron nitride was nondestructively sepa-rated from the copper substrate within 1 min. Then, the PMMA was totally dissolved by methylene chloride without the aid of any thermal annealing. To identify the residual h-BN on the SiO₂/Si substrate, AFM images were taken (shown in figure 5(a)), where we see that no obvious residues exist on the substrate surface. The room temperature opera-tion and fast transfer were the key to ensuring that the PMMA could be completely removed. The low temperature process of our method was then applied to transfer the monolayer h-BN from the copper foil onto a flexible substrate. Figure 5(b) shows the transfer onto a polyimide substrate, which can be used immediately as an epitaxial substrate. Some copper foil was slightly dissolved during the bubbling transfer process [38]. X-ray photoemission spectroscopy was used to identify the Cu residue, as shown in figure 5(c). No Cu2p$^{3/2}$ peak, which was supposed to appear from 945 to 925 eV, was identified. The absence of copper may be attributed to the rapid transfer process. It indeed appears to have many peaks, as shown in figure 5(c). Compared with figure 5(d), it clearly shows all elements could derive from the SiO₂/Si substrate except B and N. For the peaks of oxygen and carbon, we attribute them to the impurity of adsorption. This can be confirmed by identifying the carbon and oxygen residue on the SiO₂/Si substrate and h-BN/Cu foil, as shown in figures 5(d) and (e). Quantitative XPS analysis of the atomic percentage ratio was implemented at different etching time: 0 s, 50 s, and 100 s, as shown in tables S4 and S5. It clearly shows the atomic percentage ratio of the oxygen or carbon significantly reduces along with etching time. There-fore, the impurity oxygen and carbon probably derived from the adsorption in the air or in the process of detection.

4. Conclusion

In summary, by utilizing a rather simple pretreatment process, large-area (4×2 cm²), highly crystalline, and unbroken monolayer h-BN has been successfully synthesized without any surface impurities. Furthermore, we have achieved a fast, clean, and nondestructive transfer under mild conditions by

optimizing the electrochemical bubbling method. These high quality h-BN monolayer dielectrics should be a promising candidate for fabricating new types of 2D materials and even organic molecules for novel optoelectric applications.

Supporting information

Schematic diagram of the LPCVD system; AFM image of monolayer h-BN on SiO₂/Si; and SEM image of annealed copper without pretreatment and with pretreatment with acetic acid and electrochemical polishing.

Acknowledgments

References

[1] Watanabe K, Taniguchi T and Kanda H 2004 Direct-bandgap properties and evidence for ultraviolet lasing of hexagonal boron nitride single crystal *Nat. Mater.* **3** 404–9
[2] Blase X, Rubio A, Louie S G and Cohen M L 1995 Quasiparticle band structure of bulk hexagonal boron nitride and related systems *Phys. Rev.* B **51** 6868–75
[3] Hoffman D M, Doll G L and Eklund P C 1984 Optical-properties of pyrolytic boron-nitride in the energy-range 0.05–10 eV *Phys. Rev.* B **30** 6051–6
[4] Dean C R *et al* 2010 Boron nitride substrates for high-quality graphene electronics *Nat. Nanotechnology* **5** 722–6
[5] Yang W *et al* 2013 Epitaxial growth of single-domain graphene on hexagonal boron nitride *Nat. Mater.* **12** 792–7
[6] Kim E, Jain N, Jacobs-Gedrim R, Xu Y and Yu B 2012 Exploring carrier transport phenomena in a CVD-assembled graphene FET on hexagonal boron nitride *Nanotechnology* **23** 125706
[7] Okada M, Sawazaki T, Watanabe K, Taniguch T, Hibino H, Shinohara H and Kitaura R 2014 Direct chemical vapor deposition growth of WS2 atomic layers on hexagonal boron nitride *ACS Nano* **8** 8273–7
[8] Lee C-H *et al* 2014 Epitaxial growth of molecular crystals on van der Waals substrates for high-performance organic electronics *Adv. Mater.* **26** 2812–7
[9] He D *et al* 2014 Two-dimensional quasi-freestanding molecular crystals for high-performance organic field-effect transistors *Nat. Commun.* **5** 5162
[10] Zhi C, Bando Y, Tang C, Kuwahara H and Golberg D 2009 Large-scale fabrication of boron nitride nanosheets and their utilization in polymeric composites with improved thermal and mechanical properties *Adv. Mater.* **21** 2889–93
[11] Liu Z *et al* 2013 Ultrathin high-temperature oxidation-resistant coatings of hexagonal boron nitride *Nat. Commun.* **4** 2541
[12] Lindsay L and Broido D A 2011 Enhanced thermal conductivity and isotope effect in single-layer hexagonal boron nitride *Phys. Rev.* B **84** 155421
[13] Li X, Yin J, Zhou J and Guo W 2014 Large area hexagonal boron nitride monolayer as efficient atomically thick insulating coating against friction and oxidation *Nanotechnology* **25** 105701
[14] Meyer J C, Chuvilin A, Algara-Siller G, Biskupek J and Kaiser U 2009 Selective sputtering and atomic resolution imaging of atomically thin boron nitride membranes *Nano Lett.* **9** 2683–9

[15] Corso M, Auwarter W, Muntwiler M, Tamai A, Greber T and Osterwalder J 2004 Boron nitride nanomesh *Science* **303** 217–20

[16] Sutter P, Lahiri J, Albrecht P and Sutter E 2011 Chemical vapor deposition and etching of high-quality monolayer hexagonal boron nitride films *ACS Nano* **5** 7303–9

[17] Nagashima A, Tejima N, Gamou Y, Kawai T and Oshima C 1995 Electronic dispersion-relations of monerlayer hexagonal boron-nitride formed on the Ni(111) surface *Phys. Rev.* B **51** 4606–13

[18] Joshi S *et al* 2012 Boron nitride on Cu(111): an electronically corrugated monolayer *Nano Lett.* **12** 5821–8

[19] Preobrajenski A B, Vinogradov A S, Ng M L, Cavar E, Westerstrom R, Mikkelsen A, Lundgren E and Martensson N 2007 Influence of chemical interaction at the lattice-mismatched h-BN/Rh(111) and h-BN/Pt(111) interfaces on the overlayer morphology *Phys. Rev.* B **75** 245412

[20] Corso M, Greber T and Osterwalder J 2005 h-BN on Pd(110): a tunable system for self-assembled nanostructures? *Surf. Sci.* **577** L78–84

[21] Mueller F, Huefner S, Sachdev H, Laskowski R, Blaha P and Schwarz K 2010 Epitaxial growth of hexagonal boron nitride on Ag(111) *Phys. Rev.* B **82** 113406

[22] Mueller F and Grandthyll S 2013 Monolayer formation of hexagonal boron nitride on Ag(001) *Surf. Sci.* **617** 207–10

[23] Shi Y *et al* 2010 Synthesis of few-layer hexagonal boron nitride thin film by chemical vapor deposition *Nano Lett.* **10** 4134–9

[24] Song L *et al* 2010 Large scale growth and characterization of atomic hexagonal boron nitride layers *Nano Lett.* **10** 3209–15

[25] Kim K K *et al* 2012 Synthesis of monolayer hexagonal boron nitride on Cu foil using chemical vapor deposition *Nano Lett.* **12** 161–6

[26] Kim K K, Hsu A, Jia X, Kim S M, Shi Y, Dresselhaus M, Palacios T and Kong J 2012 Synthesis and characterization of hexagonal boron nitride film as a dielectric layer for graphene devices *ACS Nano* **6** 8583–90

[27] Guo N, Wei J, Fan L, Jia Y, Liang D, Zhu H, Wang K and Wu D 2012 Controllable growth of triangular hexagonal boron nitride domains on copper foils by an improved low-pressure chemical vapor deposition method *Nanotechnology* **23** 415605

[28] Tay R Y, Griep M H, Mallick G, Tsang S H, Singh R S, Tumlin T, Teo E H T and Karna S P 2014 Growth of large single-crystalline two-dimensional boron nitride hexagons on electropolished copper *Nano Lett.* **14** 839–46

[29] Frueh S, Kellett R, Mallery C, Molter T, Willis W S, King'ondu C and Suib S L 2011 Pyrolytic decomposition of ammonia borane to boron nitride *Inorg. Chem.* **50** 783–92

[30] Han J, Lee J Y, Kwon H and Yeo J S 2014 Synthesis of wafer-scale hexagonal boron nitride monolayers free of aminoborane nanoparticles by chemical vapor deposition *Nanotechnology* **25** 145604

[31] Kim G, Jang A R, Jeong H Y, Lee Z, Kang D J and Shin H S 2013 Growth of high-crystalline, single-layer hexagonal boron nitride on recyclable platinum foil *Nano Lett.* **13** 1834–9

[32] Park J-H *et al* 2014 Large-area monolayer hexagonal boron nitride on Pt foil *ACS Nano* **8** 8520–8

[33] Gorbachev R V *et al* 2011 Hunting for monolayer boron nitride: optical and Raman signatures *Small* **7** 465–8

[34] Arenal R, Ferrari A C, Reich S, Wirtz L, Mevellec J Y, Lefrant S, Rubio A and Loiseau A 2006 Raman spectroscopy of single-wall boron nitride nanotubes *Nano Lett.* **6** 1812–6

[35] Gao Y, Ren W, Ma T, Liu Z, Zhang Y, Liu W B, Ma L P, Ma X and Cheng H M 2013 Repeated and Controlled growth of monolayer, bilayer and few-layer hexagonal boron nitride on Pt foils *ACS Nano* **7** 5199–206

[36] Kim S M, Hsu A, Lee Y-H, Dresselhaus M, Palacios T, Kim K K and Kong J 2013 The effect of copper pre-cleaning on graphene synthesis *Nanotechnology* **24** 365602

[37] Wang Y, Zheng Y, Xu X, Dubuisson E, Bao Q, Lu J and Loh K P 2011 Electrochemical delamination of CVD-grown graphene film: Toward the recyclable use of copper catalyst *ACS Nano* **5** 9927–33

[38] Gao L *et al* 2012 Repeated growth and bubbling transfer of graphene with millimetre-size single-crystal grains using platinum *Nat. Commun.* **3**

[39] Li H, Wu J, Huang X, Yin Z, Liu J and Zhang H 2014 A universal, rapid method for clean transfer of nanostructures onto various substrates *ACS Nano* **8** 6563–70

[40] Wan X, Chen K and Xu J 2014 Interface engineering for CVD graphene: current status and progress *Small* **10** 4443–54